Infrared spectroscopy of NGC 4151: ISO observations and NLR line profiles

E. Sturm[1], T. Alexander[1,2,3], D. Lutz[1], A. Sternberg[2], H. Netzer[2], and R.Genzel[1]

Received 8 May 1998; accepted 25 August 1998

To appear in the Astrophysical Journal

[1]Max-Planck-Institut für Extraterrestrische Physik, Postfach 1603, D-85740 Garching, Germany

[2]Tel Aviv University, Ramat Aviv, Tel Aviv 69978, Israel

[3]Institute for Advanced Study, Olden Lane, Princeton, NJ 08540, USA

ABSTRACT

We present ISO-SWS and ISOPHOT-S spectroscopy[4] of the Seyfert galaxy NGC 4151. We detect a total of 17 fine-structure emission lines emitted by a wide range of low- and high-excitation ions, two rotational lines of molecular hydrogen, and the Brβ HI line.

We find that the mid-IR fine-structure line profiles display blue asymmetries which are very similar to those observed in the optical lines produced in the narrow line region. Because the mid-infrared lines are much less sensitive to extinction than are the optical lines this similarity places strong constraints on scenarios which have been invoked to explain the optical line asymmetries. For example, we are able to rule out the simplest radial-motion-plus-dust scenarios for the production of the line asymmetries. Our preferred model is that of a central, geometrically thin but optically thick, obscuring screen of sub-arcsecond extension, enclosing a total hydrogen gas mass of $\gtrsim 5 \times 10^6$ M$\odot$. This mass may be molecular.

The weakness of 'PAH' emission features in the low resolution spectrum is evidence that star formation plays a minor role in the circumnuclear region of NGC 4151. In a companion paper, we use the rich set of mid-infrared lines to determine the obscured photoionizing continuum produced by the active galactic nucleus.

Subject headings: galaxies: individual: NGC 4151 – galaxies: Seyfert – line: profiles – infrared: galaxies

[4]Based on observations made with ISO, an ESA project with instruments funded by ESA member states (especially the PI countries: France, Germany, The Netherlands and the United Kingdom) and with the participation of ISAS and NASA.

1. Introduction

NGC 4151 is one of the nearest (13.2 Mpc for $H_0 = 75$ km s^{-1} Mpc^{-1}, $1''$=64 pc) and best studied Seyfert galaxies (Seyfert 1943; Oke & Sargent 1968). The optical spectrum is dominated by the central non-stellar continuum source and the surrounding broad and narrow emission line regions (BLR and NLR). NGC 4151 is usually classified as a Seyfert 1 galaxy, though Osterbrock & Koski (1976) classified it as an intermediate Seyfert 1.5 system. The central source is highly variable and the broad emission lines reverberate rapidly (Penston & Pérez 1984; Ulrich et al. 1991; Edelson et al. 1996; Kaspi et al. 1996; Fernandez et al. 1997). NLR emission is produced within the inner $\sim 5''$ in a wide ionization cone (Heckman & Balick 1983; Boksenberg et al. 1995; Kaspi et al. 1996; Winge et al. 1997; Hutchings et al. 1998). The NLR is oriented along the direction of a non-thermal radio jet emanating from the nucleus (Pedlar et al. 1993). More extended ($\sim 30''$) narrow-line emission (EELR) is produced in portions of the galactic disk which are intersected by the ionization cone (Pedlar et al. 1993; Boksenberg et al. 1995). High resolution optical imaging and spectroscopic studies show that the NLR cloud dynamics are consistent with high-velocity outflows superposed on larger scale galactic disk rotation (Schulz 1990; Veilleux 1991b; Boksenberg et al. 1995; Weymann et al. 1997; Winge et al. 1997; Hutchings et al. 1998).

NGC 4151 is one of many Seyfert galaxies whose optical NLR emission lines display pronounced blue asymmetries and blue-shifts relative to the systemic velocities (e.g. Heckman et al. 1981; Veilleux 1991a,c). Such line asymmetries have generally been understood as being due to a combination of gas inflow or outflow, coupled with selective dust extinction of the red-shifted components. Mid-infrared spectroscopic observations can provide strong constraints on such models, since the mid-IR emission lines are much less sensitive to extinction than are optical lines.

In this paper we present 2.4-45 μm mid-IR spectroscopic observations of NGC 4151 carried out with the *Infrared Space Observatory (ISO)*. We focus on the remarkable similarity that we find between the shapes of the mid-IR and optical NLR line profiles. In a companion paper (Alexander et al. 1998: A98) we use our fine-structure emission line spectroscopy to determine the shape of the (obscured) continuum radiation which photoionizes the NLR in NGC 4151. Our observations are part of our program to study the mid-IR spectral properties of active galactic nuclei (AGNs), starburst galaxies, and ultraluminous infrared galaxies (Lutz et al. 1996, 1997; Kunze et al. 1996; Moorwood et al. 1996; Rigopoulou et al. 1996; Sturm et al. 1996; Genzel et al. 1998).

This paper is organized as follows. In §2 we describe our observations. In §3 we compare our mid-IR line profile observations with optical line profiles, and show that they are very similar. In §4 we use this result to argue that the line asymmetries are likely produced by a central and very optically thick obscuring screen, rather than by dust which is distributed throughout the NLR or in the emitting clouds themselves. We present a brief summary in §5.

2. Observations

We observed the central region of NGC 4151 with the Short Wavelength Spectrometer (SWS, de Graauw et al. 1996), and the spectrophotometer (ISOPHOT-S) (Lemke et al. 1996) on-board the *ISO* (Kessler et al. 1996). We also obtained a large aperture optical CCD spectrum using the Coudé Echelle spectrometer at the 2m telescope of the Karl-Schwarzschild-Observatory (KSO, Landessternwarte Thüringen). We use the optical observations in our comparison analysis described in §3.

Our SWS observations were carried out during revolution 172 (1996 May 7). We obtained a full grating scan (SWS01 speed 1 mode - $\lambda/\Delta\lambda \approx 250...600$) from 2.4 to 45 μm as well as a large set of individual line scans (SWS02 mode - $\lambda/\Delta\lambda \approx 1000...2500$). The full grating scan is relatively noisy, and we do not present it here. The average total integration time per individual line scan was 1200 seconds. We reduced our spectra using the SWS Interactive Analysis System (SIA) (Lahuis et al. 1998, Wieprecht et al. 1998,). We adopted the September 1997 flux calibration.

Our individual line spectra are shown in Figure 1. We detected 17 fine-structure emission lines from a wide range of ionic species, two pure rotational lines of molecular hydrogen (H_2) and the Brβ HI recombination line. Table 1 lists the measured line fluxes, as well as upper limits for several undetected lines. The error estimates on observed fluxes in Table 1 are based on the uncertainty in defining the underlying continuum. In addition there is a general flux calibration uncertainty of $\approx$20% (Schaeidt et al. 1996). The SWS aperture sizes range between $14'' \times 20''$ and $20'' \times 33''$. Yoshida and Ohtani (1993) showed that more than 80% of the [OIII] and [OII] optical line flux of the NLR plus EELR is produced within the inner ∼4"x4" region. Therefore, we can safely assume that we have detected all of the mid-IR emission from the NLR and most of the EELR. This is illustrated in Figure 2, in which the SWS apertures are overlayed on the [O III] λ5007 contours of the NGC 4151 nucleus (adapted from Yoshida & Ohtani 1993). We do not apply aperture correction factors to the measured line fluxes in our analysis.

As shown in Table 1 the observed fine-structure lines are emitted by ions with excitation energies which range from 8 to 303 eV. The high-excitation coronal lines are unambiguous diagnostics of non-stellar photoionization (Oliva et al. 1994, Ferguson et al. 1997). In A98 we use the fluxes listed in Table 1 together with photoionization models to determine the spectral shape of the Lyman continuum radiation field which is photoionizing the NLR. As discussed in A98 the density sensitive flux ratios of the [NeV] 14.32, 24.32 μm, [NeIII] 15.55,36.04 μm, and [SIII] 18.71,33.48 line pairs, in combination with the [O III] 51.81, 88.35 μm pair (Spinoglio et al. 1998), imply an NLR electron density of ~ 1000 cm^{-3}. The optical to mid-IR flux ratio [NeIII] 3868Å/15.55μm implies an electron temperature of 13000 ± 2500 K for the NLR gas, assuming a reddening of E_{B-V} = 0.05-0.15 (see A98). The continua in our spectra agree well with the IRAS fluxes, but do not indicate a pronounced bimodal dust emission as proposed by Rodriguez-Espinosa et al. (1996).

Our ISOPHOT-S observations were carried out during revolution 234 (1996 August 2). These observations provided a low-resolution ($\lambda/\Delta\lambda \approx 90$) spectrum between 2.5 to 11.6 μm. We processed the data using the ISOPHOT Interactive Analysis (PIA) software[5], version 6.0. Our ISOPHOT-S spectrum of NGC 4151 is displayed in Figure 3.

ISOPHOT-S spectra are ideally suited for studying emission features produced by 'large molecules' such as the Polycyclic Aromatic Hydrocarbons (PAHs). Such emission features trace star-formation regions and are weak or absent in AGNs (Roche et al. 1991, Genzel et al. 1998). In NGC4151 we do not detect any PAH features. We determined upper limits to the PAH fluxes at 6.2μm and 7.7μm by first subtracting a continuum set by a linear interpolation between the fluxes at 5.9μm and 10.95μm, and then integrating the spectrum from 6.0 to 6.5 and 7.3 to 8.2 μm. We derive upper limits of 2.5e-19 and 3.7e-19 W/cm^2 for the 6.2μm and 7.7μm PAH fluxes. These limits imply that starburst regions contribute at most 20% to the production of the low-ionization fine-structure lines in NGC 4151 (see A98). Our optical spectral observations were carried out with the KSO Coudé Echelle Spectrometer during several nights between 6th and 10th of February 1998. We used the UV Prism (3600 - 5300 Å) and a slit size of $6.8'' \times 15''$, corresponding to a spectral resolution of about 10000. The position angle for the different observations varied between 0 and 40 degrees. We coadded 4 spectra of 1800 seconds exposure time each. Our goal was to obtain a high quality large aperture spectral scan of the [OIII] 5007 Å emission line. Our result is shown in Figure 4.

[5]PIA is a joint development by the ESA astrophysics Division and the ISOPHOT Consortium led by the Max Planck Institut für Astronomie (MPIA), Heidelberg. Contributing ISOPHOT Consortium institutes are DIAS, RAL, AIP, MPIK and MPIA.

3. Line Profiles

An inspection of Figure 1 shows that all of the detected fine-structure emission lines are asymmetric, with excess emission clearly visible on the blue sides of the lines. On average the flux under the red wing of the line profiles is 80% of the blue wing flux. In Table 1 we quantify these asymmetries by listing the line center velocities (C50, e.g. Heckman et al. 1981) defined at 50% of the peak intensities, relative to the systemic velocity of 1000 km s^{-1} (Schulz 1990). All of the line-center velocities are negative indicating a blue-shifted bias in the emission lines. We find a mean value $< C50 >= -44 \pm 20$ km s^{-1} for the mid-IR lines listed in section 1.

Blue asymmetries are well known features of the optical narrow emission lines in many Seyfert galaxies, including NGC 4151. Our observations reveal, for the first time, similar asymmetries in the mid-IR emission lines. A key question which we now wish to address is: How similar are the mid-IR profiles to the optical emission line profiles?

Many optical emission line observations of NGC 4151 have been presented in the literature. These include the ground-based imaging and spectroscopic studies by Walker (1968a,b), Ulrich (1973), Heckman et al. (1981), Pelat & Alloin (1982), Schulz (1987, 1990) and Veilleux (1991a,b,c), and the more recent *HST* observations by Evans et al. (1993), Boksenberg et al. (1995), Winge et al. (1997) and Hutchings et al. (1998). The biconical structure of the NLR in NGC 4151 was already apparent in Walker's and Ulrich's observations. Indeed, the four major [OIII] emission complexes identified by Ulrich (see her Figure 4) are discernable (at much higher resolution) in the recent *HST* STIS image presented by Hutchings et al. Heckman et al. (1981) carried out a long-slit spectroscopic survey of [OIII] λ 5007Åemission in a sample of Seyfert galaxies and found that most of the lines in their sample display significant blue asymmetries. In NGC 4151 they found that C50=-90 km s^{-1} relative to the systemic velocity. Pelat & Alloin (1982) carried out high-resolution ($\sim$ 15 km s^{-1}) observations of the [OIII] 5007Å line with it's prominent blue shoulder. Similar high-resolution observations were carried out by Schulz (1987), who observed (narrow) Hα and Hβ and the [NII] $\lambda\lambda 6548, 6583$, [SII] $\lambda 6716, 6731$ and [OI] $\lambda 6300$ lines in addition to the [OIII] doublet. Schulz found an [OIII] profile very similar to that measured by Pelat & Alloin, and found that $< C50 >= -37 \pm 6$ km s^{-1} averaged over the lines he observed, in good agreement with the mean value of the *ISO* mid-IR lines. More recently, Veilleux (1991a) carried out $\sim$ 10 km s^{-1} resolution and $2.5'' \times 2.5''$ aperture optical observations of several Seyferts. For NGC 4151 Veilleux presented profile observations of Hα, Hβ and the [OI], [OIII], [SII], and [NII] lines, and also the (narrow) HeI $\lambda 5876$, HeII $\lambda 4686$ lines, as well as the [ArIII]

λ7136, [FeVII] λ5721, and [FeVIII] λ5721 lines (see his Figure 14). All of the lines of NGC 4151 displayed by Veilleux (1991a) show blue asymmetries similar to those found by Pelat & Alloin and Schulz, though there are small differences in detail between the different lines.

Here we compare our mid-IR spectra to the optical line profiles presented by Veilleux (1991a). These optical observations are spatially integrated over the central $\sim 3''$, which is small compared to the SWS apertures. However, our large aperture [O III] 5007Å spectrum (Figure 4), is almost identical to the spectrum presented by Veilleux (see also Figures 5a and b). This demonstrates that our ISO observations are likely sampling the same regions giving rise to the optical line profiles.

Three further considerations are required in this comparison. First, with the exception of [ArIII] 8.99 μm, the mid-IR fine-structure lines are not emitted by the same ions which emit the optical forbidden lines. However, emission lines from neighboring ionization states of the same element are available in the combined mid-IR and optical data set. We therefore chose to compare the profiles of the optical/mid-IR line pairs [OIII]5007Å/[OIV]25.89μm, [SII]6716Å/[SIII]18.71μm, [SII]6716Å/[SIII] 33.48μm, [SII]6716Å/[SIV]10.51, and [ArIII]7136Å/[ArIII]8.99μm. Second, correlations between the profile shapes and the ionization level, gas temperature, and transition critical densities could introduce intrinsic differences between the optical and mid-IR emission lines. In NGC 4151 such correlations appear to be very weak, and the evidence is controversial (Veilleux 1991c, Schulz 1990). No such correlations are apparent in our ISO observations. This supports the conclusions of Veilleux (1991b) that the line shapes do not depend on the ionization potentials or the critical densities of the transitions. Third, the SWS spectral resolution is much lower than the resolution of the optical measurements. We therefore convolved the [O III], [S II], and [Ar III] optical lines with the appropriate ISO instrumental profiles at the wavelengths of the [O IV], [S III], [SIV] and [ArIII] fine-structure lines. The instrumental SWS profiles are well approximated by a Gaussian, and the variation of profile width with wavelength is known (Valentijn et al. 1996a). The instrumental profile depends on the source extension, but because the NLR is compact compared to the SWS aperture we treated the NLR as a point source.

The result of our optical-infrared comparison is shown in Figure 5. It is immediately apparent that the optical and mid-IR profiles are very similar. Differences between the profiles are no larger than 5-10% (see the residual plots in each panel of Figure 5). As shown above the average line center velocities ($< C50 >$) are identical within the uncertainties. Panels a and b demonstrate the equivalence of the Veilleux (1991a) data with large aperture data. The prominent shoulders in the optical profiles are smeared out somewhat when smoothing to the lower SWS resolution, but the profiles still display pronounced blue asymmetries, as do the mid-IR lines. In the next section we argue that the remarkable similarities between the optical and mid-IR profiles point to a specific origin for the blue asymmetries.

4. Discussion

The simplest models of optical line profile asymmetries in Seyfert galaxies invoke spherically symmetric outflows or inflows, combined with extended dust extinction through the NLR or dusty emission line clouds (Heckman et al. 1981; Dahari & De Robertis 1988; De Robertis & Shaw 1990). In outflow models, the outwardly moving clouds are embedded in an extended dusty NLR with a total line-of-sight visual extinction $A_V \sim 1$. Red-shifted emission is produced by clouds on the far-side and is attenuated relative to blue-shifted emission on the near-side of the NLR. In inflow models, the NLR is assumed to be optically thin, but each of the individual inflowing emission-line clouds are dusty with $A_V \sim 1$. In this picture, the blue-shifted clouds are on the far-side of the NLR and are visible because their illuminated sides face the observer. Red-shifted emission is produced on the inflowing clouds on the near-side of the NLR, but is attenuated by the dust within the clouds. However, because $A_V \approx 50A_{mid-IR}$ neither of these models are compatible with our finding that the optical and mid-IR lines display almost identical blue asymmetries. The $A_V \sim 1$ required to produce an asymmetry in the optical lines, without completely blocking the red-shifted emission, would have negligible distorting effect on the mid-IR lines. Further, for any value of A_V one would expect the mid-IR lines to show less asymmetry than the optical lines.

Alternatively, the blue asymmetries could be produced by very optically thick material which is opaque at both optical and mid-IR wavelengths, and which fully blocks some of the more distant NLR emission from view (Whittle 1985; Dahari & De Robertis 1998; Veilleux 1991c; Quintilio & Viegas 1997). This possibility is consistent only with outflowing gas, where the blue-shifted material is on the near-side of the NLR. This scenario is strongly favored by our observations, since identical optical and mid-IR line profiles would then be expected.

Are the blue-shifted NLR clouds in NGC 4151 outflowing? Hutchings et al. (1998) found that many of the high-velocity blue-shifted [OIII] emission line clouds they observed are moving at velocities very close to the velocity of the blue-shifted [CIV] absorption features present in the UV spectrum of NGC 4151 (Weymann et al. 1997). As noted by Hutchings et al. (1998) this strongly suggests that the blue-shifted clouds are outflowing and are on the near-side of the NLR.

An occulting gas mass may be estimated from the assumption that the NLR outflow in NGC 4151 is approximately symmetric, and that about 20% of the red-shifted counterparts to the high velocity blue-shifted clouds are blocked from view, in order to reproduce the observed line asymmetry. The blue-shifted high velocity clouds are located within distances of the order $1''$ to $2''$ of the nucleus on the SW side of the NLR cone, with the highest velocity clouds closest to the nucleus (Hutchings et al. 1998; Ulrich 1973). We approximate the cone as having constant surface brightness in the lines. We hence estimate that, to obscure 20% of the red-shifted emission, a region of (projected) radius $\sim 0.7''$ has to be blocked by opaque material ($(0.7''/1.5'')^2 \sim 0.2$), perhaps in the form of a disk or a torus which is perpendicular to the jet axis. For this disk or torus to be opaque in the mid-IR its thickness must correspond to a hydrogen column density of $\gtrsim 10^{23}$ cm^{-2} assuming a Galactic gas-to-dust ratio. The total mass is then $\gtrsim 5 \times 10^6$ $M_\odot$. This is a lower limit, because we did not consider de-projection of the radius of the obscuring disk and because the column density could be much higher. The lower limit for the occulting gas mass is fully consistent with the 2.4x10^7 solar masses inferred from millimetre CO measurements by Rigopoulou et al. (1997) within a $23''$ beam (assuming a Galactic CO/H_2 conversion factor). Thus the obscuring material could be molecular.

We note that (at least part of) the rotational H_2 emission we have observed could be produced in this obscuring mass. The line width (FWHM) of the two detected H_2 lines is approximately 230 km/s. Such a velocity, interpreted as virial flow in a compact region of radius 46 pc, translates into a central mass of 2.7x10^8 $M_\odot$. This is an approximate but plausible central mass in view of recent results from reverberation mapping (Edelson et al 1996), and also compared to the total enclosed masses within the central 50 pc regions of other galaxies, including the Milky Way (e.g. Genzel, Hollenbach & Townes, 1994). The rotational H_2 lines trace warm gas at temperatures of $\sim$100 K and higher. For thermal emission the ratio of the S(1) and S(0) lines is approximately $112\exp(-505/T)$ where T is the gas temperature (K). Our observed lower limit of 2.4 for this flux ratio implies a minimum temperature of 130 K for the S(1) emitting gas. At this temperature the observed S(1) flux corresponds to a (maximum) warm H_2 mass of 3×10^7 $M_\odot$. At temperatures closer to 200 K, that appear plausible from observations of other galaxies (Rigopoulou et al. 1996, Valentijn et al. 1996b), the warm H_2 mass would be $\sim 3 \times 10^6$ $M_\odot$. This suggests that the bulk of the obscuring material may be warm.

It is, of course, possible that the observed anisotropic distribution of the line emitting clouds is real, i.e. there could simply be more bright, blue shifted clouds close to the nucleus than red shifted ones, giving rise to identical optical and mid-IR line asymmetries. However, it would be difficult to reconcile such an idea with the preferential blueshift and blueward asymmetry also found in many other Seyferts (e.g. Heckman et al. 1981, Veilleux 1991b).

5. Conclusions

We have obtained ISO SWS and ISOPHOT-S spectra of the NLR of the Seyfert galaxy NGC 4151. We detect 17 fine structure emission lines, as well as two lines of molecular hydrogen (0-0 S(1) and S(5)) and one hydrogen recombination line (Brβ). In addition we derived upper limits for 4 further fine structure lines, and H_2 S(2) and S(0). The emission lines span a wide range of ionization potential (8-303 eV), tracing the ionizing UV radiation in a wavelength range that has barely been accessible before.

The PAH features are absent within our detection limit. The upper limits we derive for the features at 6.2 and 7.7 μm confirm that there is no significant starburst contribution to the total luminosity of the nuclear region.

The emission line profiles are asymmetric (in the sense of a blue excess) and blue shifted with respect to the sytemic velocity. We have compared the ISO line profiles to optical, high resolution profiles. The profiles are very similar, reproducing the same asymmetries and blue shifts. Since the infrared lines are much less sensitive to extinction, this means that simple dust-plus-radial-motion models cannot explain the observed profiles.

Two alternative models remain plausible: a real anisotropic distribution of the line emitting clouds, and an obscuring screen close to the nucleus. The first alternative might be a good explanation for a few individual objects. In larger samples, however, this effect should average out. Our prefered model is that of a geometrically thin but optically thick obscuring screen of (projected) sub-arcsecond extension, enclosing a total mass of $\gtrsim 5 \times 10^6$ M$\odot$. These dimensions are consistent with HST imaging and millimetre CO measurements. The obscuring mass may be primarliy molecular and the source of the H_2 rotational emission we have observed.

Our study demonstrates the value of optical-infrared line profile comparisons and the potential of applying this method to other Seyfert galaxies observed with ISO-SWS.

We are grateful to Henrik Spoon for providing us with the reduced ISOPHOT-S spectrum and PAH flux measurements. We also thank Eike Günther for taking the Tautenburg (KSO) spectrum, and Thomas Gehren for providing software and assistance with the reduction of it. We thank Mike Eracleous for dicussion. This work was supported by DARA under grants 50-QI-8610-8 and 50-QI-9492-3, and by the German-Israeli Foundation under grant I-196-137.7/91.

REFERENCES

Alexander, T., Sturm, E., Lutz, D., Sternberg, A., Netzer, H. and Genzel, R. 1998, submitted to ApJ(A98)

Boksenberg A., et al. 1995, ApJ, 440, 151

Cameron, M., Storey, J.W.V., Rotaciuc, V., et al. 1993, ApJ, 419, 136

Dahari, O.A., and De Robertis, M.M. 1988, ApJ, 331, 727

de Graauw, T. et al. 1996, A&A, 315, L49

De Robertis M.M., and Osterbrock D.E. 1984, ApJ, 286, 171

De Robertis M.M., and Shaw, R.A. 1990, ApJ, 348, 421

Edelson, R., et al. 1996, ApJ, 470, 364

Evans, I.N., Tsvetanov, Z., Kriss, G.A., et al. 1993, ApJ, 417, 82

Ferguson, J.W., Korista, K.T., and Ferland, G.J. 1997, ApJS, 110,287

Genzel R., Hollenbach, D., and Townes, C.H. 1994, Rep.Progr.Phys. 57,417

Genzel R., Lutz, D. Sturm, E. et al. 1998, ApJ, in press

Heckman, T.M., and Balick, B. 1983, ApJ, 268, 102

Heckman, T.M., Miley, G.K., van Breugel, J.M. and Butcher, H. 1981, ApJ, 247, 403

Hutchings, J.B., Crenshaw, D.M., Kaiser, M.E., et al. 1998, ApJ, 492, L115

Kaspi, S., et al. 1996, ApJ, 470, 336

Kessler, M.F., Steinz, J.A., Anderegg, M.E. et al. 1996, A&A, 315, L27

Knop, R.A., Armus, L., Larkin, J.E. et al. 1996, AJ, 112, 81

Kunze, D., et al. 1996, A&A, 315, L101

Lahuis, F., Wieprecht, E. and Sturm, E. 1998, 'Proceedings of the ADASS97 Conference', ASP Conference Series, in press

Lemke D., et al. 1996, A&A, 315, L64

Lutz D., Genzel, R., Sternberg, A. et al. 1996, A&A, 315, L137

Lutz, D., Sturm, E., Genzel, R., Moorwood, A.F.M., and Sternberg, A. 1997, Ap&SS, 248, 217

Moorwood A. F. M., et al. 1996, A&A, 315, L109

Oke, J.B., and Sargent, W.L.W., ApJ, 151, 807

Oliva, E., Salvati, M., Moorwood, A.F.M., Marconi, A. 1994, A&A, 288, 457

Osterbrock, D.E., and Koski, A.T. 1976, MNRAS, 176, 61P

Pedlar, A., et al. 1993, MNRAS, 264, 471

Pelat, D. and Alloin, D. 1982, A&A, 105, 335

Penston, M.V., and Pérez, E. 1984, MNRAS, 211, 33P

Quintilio, R., and Viegas, S.M. 1997, ApJ, 474, 616

Rigopoulou, D., et al. 1996, A&A, 315, L125

Rigopoulou, D., Papadakis, I., Lawrence, A., and Ward, M. 1997, A&A, 327, 493

Roche, P.F., Aitken, D.K., Smith, C.H., and Ward, M.J. 1991, MNRAS, 248, 606

Rodriguez-Espinosa, J.M., Perez Garcia, A.M., Lemke, D., and Meisenheimer, K. 1996, A&A, 315, L129

Schulz H. 1987, A&A, 178, 7

Schulz H. 1990, AJ, 99, 1442

Schaeidt S. G., et al. 1996, A&A, 315, L55

Seyfert, C.K. 1943, ApJ, 97, 28

Spinoglio, L., et al. 1998, in: 'Extragalactic Astronomy in the Infrared', G.A. Mamon, Trin Xuân Thuân, J. Trân Thanh Vân (eds.), Editions Frontières, Gif-Sur-Yvette

Sturm, E., et al. 1996, A&A, 315, L133

Ulrich, M.H. 1973, ApJ, 181, 51

Ulrich, M.H., Boksenberg, A., Penston, M.V., Bromage, G.E., Claevel, J., Elvius, A., Perola, G.C., Snijders, M.A.J. 1991, ApJ, 382, 483

Valentijn, E.A., Feuchtgruber, H., Kester, D.J.M. et al. 1996a, A&A, 315, L60

Valentijn, E.A., van der Werf, P.P, de Graauw, T., and de Jong, T. 1996b, A&A, 315, L145

Veilleux S., 1991a, ApJS, 75, 357

Veilleux S., 1991b, ApJS, 75, 383

Veilleux S., 1991c, ApJ, 369, 331

Walker, M.F. 1968a, AJ, 73, 854

Walker, M.F. 1968b, ApJ, 151, 71

Weymann, R.J., Morris, S.L., Gray, M.E., and Hutchings, J.B. 1997, ApJ, 483, 717

Whittle, M. 1985, MNRAS, 216, 817

Wieprecht, E. et al. 1998, 'Proceedings of the ADASS97 Conference', ASP Conference Series, in press

Winge, C., Axon, D.J., Macchetto, F.D., and Capetti, A. 1997, ApJ, 487, 121

Yoshida M., and Ohtani H. 1993, PASJ, 45, 407

This manuscript was prepared with the AAS LaTeX macros v4.0.

Fig. 1.— The SWS line spectra of NGC 4151

Fig. 2.— The ISO-SWS aperture position superimposed on the [O III] λ5007 contours of the NGC 4151 nucleus (adapted from Yoshida & Ohtani 1993). The interval between the solid contour lines is 1 magnitude. The dotted contour is 8.5 magnitudes weaker than the central contour. The rectangles represent the $14'' \times 20''$ and $20'' \times 33''$ – i.e. the smallest and largest – aperture of SWS.

Fig. 3.— The ISOPHOT-S spectrum of NGC 4151 (long wavelength part only). The dominant pixel at 10.5 μm is the [S IV] line. There is no indication for strong PAH features at 6.2, 7.7, 8.7 or 11.2 μm, and hence no indication for a strong contribution of a starburst component.

Fig. 4.— Large aperture [O III] 5007Å spectrum of NGC 4151.

Fig. 5.— Comparison of the ISO SWS line profiles (solid lines) with their optical counterparts convolved with the SWS instrumental profile (dashed). The optical lines are taken from: a: The KSO Tautenburg [O III] 5007Å spectrum. b: [O III] 5007Å of V91a. c,d,e,f: [Ar III] and [S II] of V91a. The lower part of each panel shows the difference (ISO - optical) of the two profiles. +10% and -10% margins in the residual plots are shown as horizontal dashed lines. Units are: velocity (km/s) with respect to the peak (x-axis), and normalized flux densities (y-axis).

Table 1: Observed line fluxes, profile widths, and velocity shifts.

Line	λ_0	$E_{\rm ion}$[a]	f_ℓ[b]	Δf_ℓ[c]	FWHM[d]	C50[e]
	μm	eV	10^{-13} erg s^{-1} cm^{-2}		km s^{-1}	km s^{-1}
[Si IX]	2.584	303.2	0.23	0.05	?	?
Brβ	2.625	13.6	0.47	0.01	?	?
[Mg VIII]	3.028	224.9	0.62	0.04	258	-22
[Si IX]	3.935	303.2	0.41	0.01	170	-29
[Mg IV]	4.487	80.1	0.31	0.02	?	?
H_2 S(5)	6.910	—	0.85	0.05	235	-76
[Ne VI]	7.652	126.2	7.83	0.04	281	-25
[Ar III]	8.991	27.6	2.2	0.1	357	-79
[S IV]	10.511	34.8	11.3	0.1	354	-24
[Ne II]	12.814	21.6	11.8	0.1	318	-48
[Ne V]	14.322	97.1	5.5	0.5	288	-44
[Ne III]	15.555	41.0	20.7	0.2	346	-51
H_2 S(1)	17.035	—	1.20	0.15	227	-22
[S III]	18.713	23.3	5.4	0.01	431	-24
[Ne V]	24.317	97.1	5.59	0.05	376	-68
[O IV]	25.890	54.9	20.3	0.2	451	-83
[Fe II]	25.988	7.9	0.44	0.02	447	-23
[S III]	33.480	23.3	8.1	0.5	?	?
[Si II]	34.815	8.2	15.6	0.9	352	-42
[Ne III]	36.013	41.0	3.5	0.1	?	?
[Mg VII]	5.50	186.5	<1.0	—	—	—
[Mg V]	5.610	109.2	<1.5	—	—	—
H_2 S(2)	12.279	—	<1.2	—	—	—
[Fe III]	22.925	16.2	<0.2	—	—	—
[Fe I]	24.042	0.0	<0.4	—	—	—
H_2 S(0)	28.219	—	<0.5	—	—	—
PAH	6.2	—	<25.0	—	—	—
PAH	7.7	—	<37.0	—	—	—

[a] Ionization potential of the stage leading to the transition.

[b] Observed flux.

[c] Error estimate on observed flux, based only on the uncertainty in defining the underlying continuum. In addition there is a general flux calibration uncertainty of ≈20%.

[d] Observed width, i.e. without deconvolution of the instrumental profile. Note that the FWHM of the instrumental profile ranges between 120 and 300 km/s.

[e] The unweighted mean velocity of the profile at half maximum relative to the systemic velocity of 1000 km s^{-1} (Schulz 1987). Question marks mean that the profile parameters could not be determined reliably.

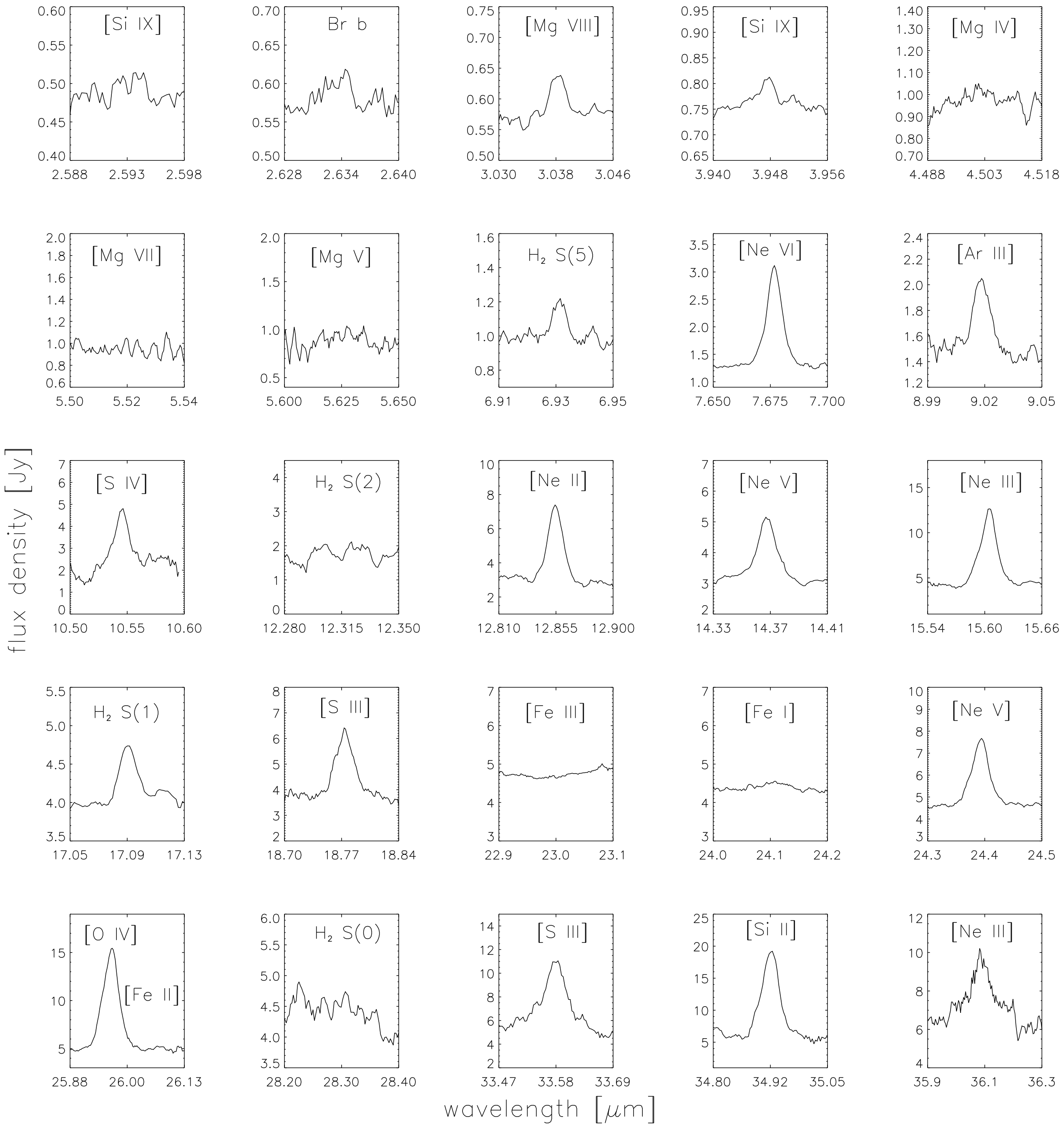
[Si IX]
Br b
[Mg VIII]
[Si IX]
[Mg IV]
[Mg VII]
[Mg V]
H2 S(5)
[Ne VI]
[Ar III]
[S IV]
H2 S(2)
[Ne II]
[Ne V]
[Ne III]
H2 S(1)
[S III]
[Fe III]
[Fe I]
[Ne V]
[O IV]
[Fe II]
H2 S(0)
[S III]
[Si II]
[Ne III]
flux density [Jy]
wavelength [μm]

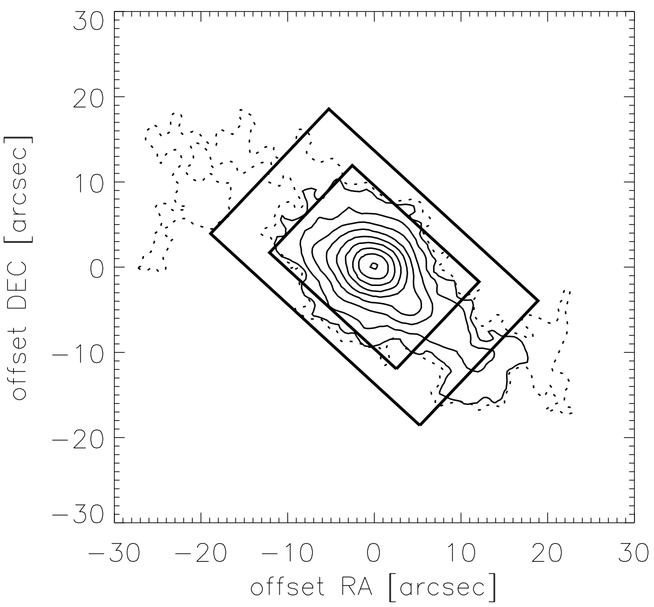

30
20
10
0
−10
−20
−30
offset DEC [arcsec]
−30
−20
−10
0
10
20
30
offset RA [arcsec]

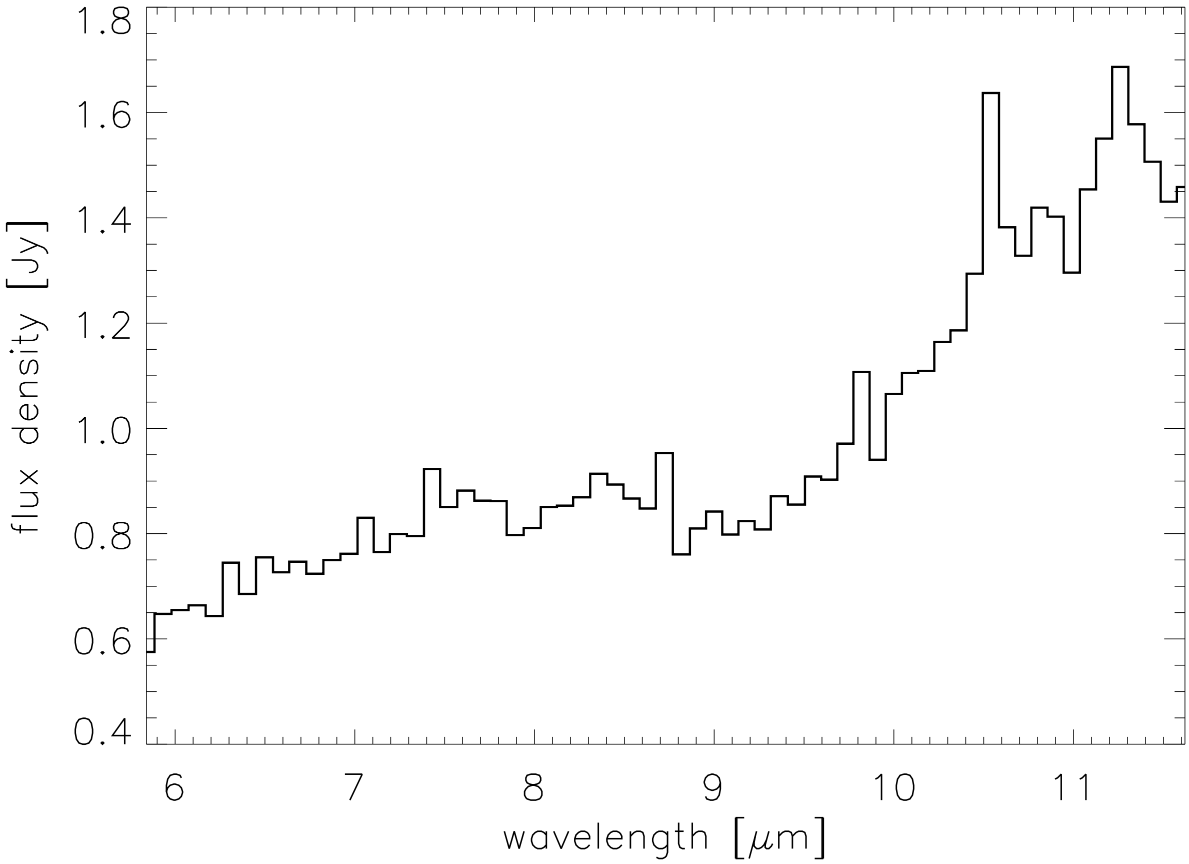

1.8
1.6
1.4
1.2
1.0
0.8
0.6
0.4
flux density [Jy]
6
7
8
9
10
11
wavelength [μm]

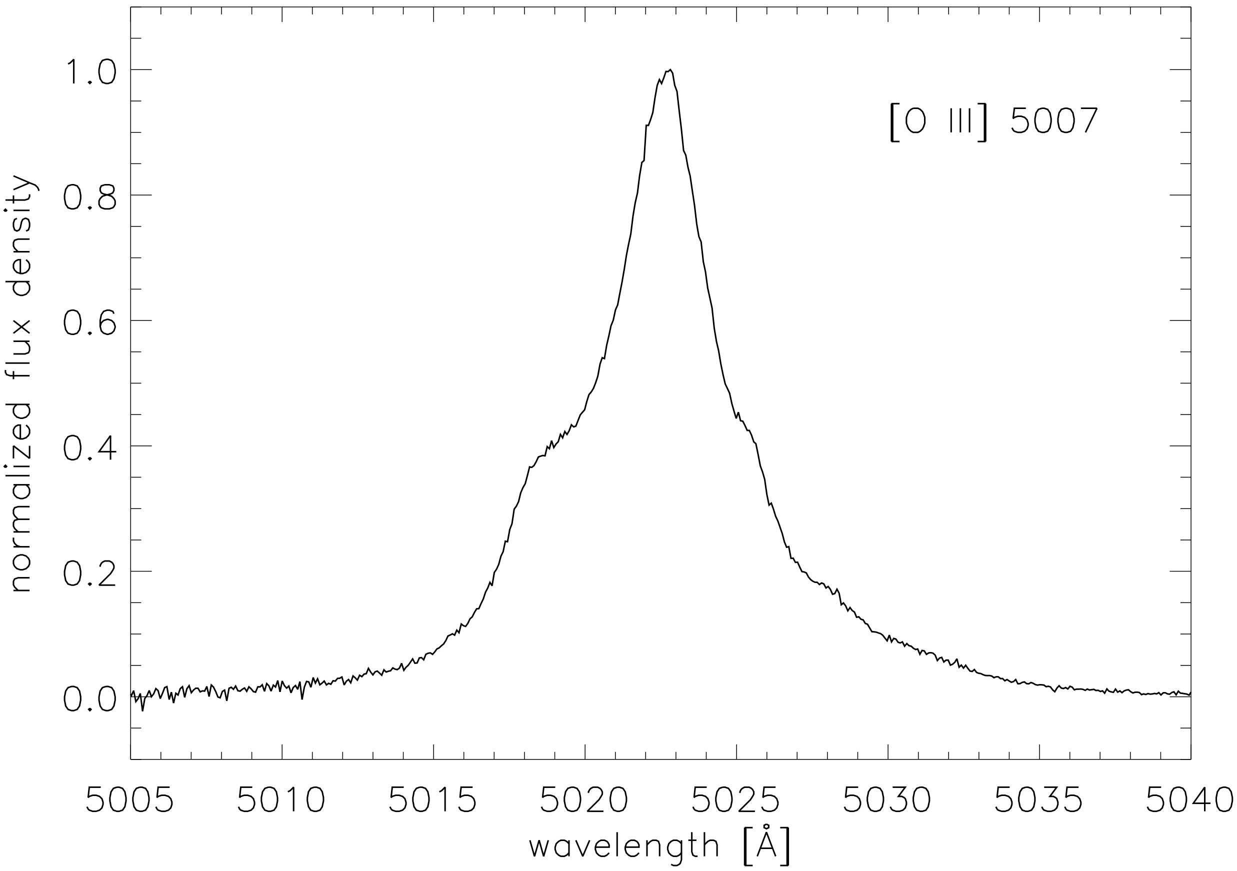

[O III] 5007
normalized flux density
0.0
0.2
0.4
0.6
0.8
1.0
5005
5010
5015
5020
5025
5030
5035
5040
wavelength [Å]

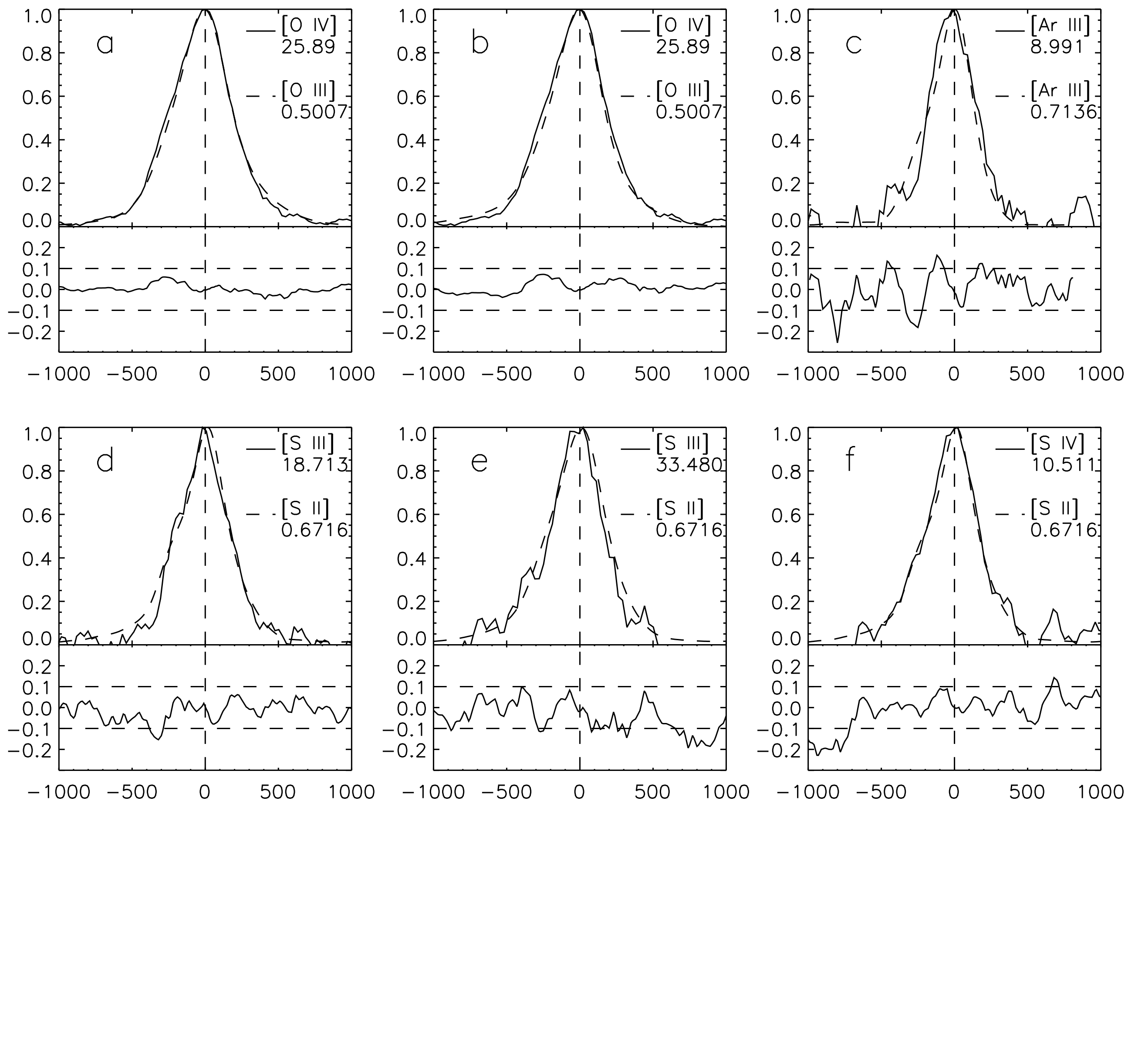
a
b
c
d
e
f
[O IV] 25.89
[O III] 0.5007
[Ar III] 8.991
[Ar III] 0.7136
[S III] 18.713
[S III] 33.480
[S IV] 10.511
[S II] 0.6716